DINAME 2017 - Proceedings of the XVII International Symposium on Dynamic Problems of Mechanics
A. T. Fleury, D. A. Rade, P. R. G. Kurka (Editors), ABCM, São Sebastião, SP, Brazil, March 5-10, 2017

Instability Prediction and Rotordynamic with Seals: Simulations Based on the Bulk-Flow Theory and Experimental Measurements

Christian Wagner[1], **Wataru Tsunoda**[2], **Tobias Berninger**[1], **Thomas Thümmel**[1] **and Daniel Rixen**[1]

[1] Chair of Applied Mechanics, Technical University of Munich, Boltzmannstrasse 15, 85748 Garching, {c.wagner, t.berninger, thuemmel, rixen}@tum.de

[2] Department of Mechanical Engineering,Tokyo Institute of Technology, 4259, Nagatsuta-cho, Midori-ku, 226-8503 Yokohama, Japan, tsunoda.w.aa@m.titech.ac.jp

Abstract: In high-speed rotational machinery such as pumps or compressors, contactless seals are commonly used to separate different fluids or gases and pressure levels. However, the presence of a leakage flow through the seal gap exerts forces on a moving, vibrating rotor. These can culminate in stiffening, restoring, and damping effects as well as in unstable, self-excited vibrational behavior. The JEFFCOTT *rotor model and rotordynamic seal coefficients are put under investigation to prevent instability in the rotating machinery and to determine the rotor-seal system's dynamic behavior. Two different methods are shown: an experimentally based one–on which this paper focuses–and a simulation-based one using simple, well known models of bulk-flow theory. The experimental method is examined on a flexible rotor-seal test rig using an active magnetic bearing for excitation. Coefficient identification problems due to unknown random force (noise) in the experimental case are shown and a solution is described in detail and validated on the test rig. Both methods lead to a calculation of rotordynamic seal coefficients during safe operating conditions. They are ultimately used to describe the system's behavior and to predict the onset speed of instability using extrapolation techniques.*

Keywords: rotordynamic, seal, instability, self-excited vibration, active magnetic bearing, coefficient measurement

INTRODUCTION

Seals in turbopumps are mostly used to minimize leakage flow from high pressure areas to low pressure parts. Because of the high rotational speeds of common centrifugal pumps or compressors, contactless seals, such as floating ring, labyrinth or small gaps are inserted between the rotating and the stationary parts. The ever-present clearance around these contactless seals permits fluid flow through the gap. For an eccentric rotor position, the fluid-velocity distribution inside the seal becomes unsymmetrical, which entails forces on the rotor. These can induce effects such as stiffening, damping, and added mass, but they can also end up in a rotor instability, a self-excited vibration which can destroy the machinery. Seal effects can engender the critical speeds that should be avoided in stationary operation. Thus, dry predictions of the rotor-system's behavior, such as those for critical speeds, damping or stability limits, are unusable under real operating conditions.

The seal forces within a rotor system are mostly modeled as rotordynamic coefficients:

$$-\mathbf{h}_s = \begin{bmatrix} m_{xx} & 0 \\ 0 & m_{yy} \end{bmatrix} \ddot{\mathbf{q}} + \begin{bmatrix} c_{xx} & c_{xy} \\ c_{yx} & c_{yy} \end{bmatrix} \dot{\mathbf{q}} + \begin{bmatrix} k_{xx} & k_{xy} \\ k_{yx} & k_{xx} \end{bmatrix} \mathbf{q} \tag{1}$$

with the motion of the rotor, $\mathbf{q}$, the seal reaction force, $\mathbf{h}_s$, and the rotordynamic seal coefficients m, c and k for added mass, the fluid's inertia, damping, and stiffness with cross-coupling parts. The coupling inertia terms in the mass matrix are neglected. The different types of seals in a pump can usually be simplified to a cylindrical annular seal for a rotordynamic analysis.

To ensure safe rotor-seal system operation, validated models and methods for characterizing the seals' behavior, the rotordynamic seal coefficients, in simulation and experiment are needed.

LITERATURE OVERVIEW

The prediction of seal forces and effects mostly leads to a calculation of their rotordynamic coefficients. Several efforts have been made for theoretical and experimental prediction. Simple and fast models are based on bulk-flow theory, which is a simplification of the NAVIER-STOKES equations assuming a constant fluid velocity along the seal's clearance.

One of the first efforts to determine restoring seal forces was made by (Black and Jenssen, 1969). They used the bulk-flow theory and incompressible fluid flow through a short annular seal. They express equilibrium through the axial momentum equation using turbulent wall friction models and the given pressure gradient over the seal as a boundary condition. For a centered rotor position, a perturbation analysis with small dynamic motion results in differential equations

of the fluid's motion. Moreover, a linearization of the fluid forces in reaction to the perturbation leads to the rotordynamic seal coefficients for the centered shaft position. The circumferential flow is supposed to be a fully developed, turbulent COUETTE flow. The assumption of constant fluid velocity in the axial and circumferential directions leads to a constant wall-friction factor, λ, for the whole seal (Barrett, 1984).

Also based on the bulk-flow theory, (Childs, 1983) introduced a closed-form analytical solution for the rotordynamic coefficients of a short, plain annular seal. He also used a perturbation analysis to solve the differential equations. The model's improvement is the consideration of fluid inertia terms and the inlet swirl, the circumferential fluid velocity at the seal's entrance; see (Barrett, 1984). The simulation agrees well overall with measurements; see (Tiwari et al., 2005).

(Padavala and Palazzolo, 1994) developed another, more detailed model, but with higher computational costs. Based on bulk-flow theory, the model discretizes the annulus into finite parts to consider a variation of wall-friction factors in the circumferential and axial directions. In contrast to the finite difference methods used in (Dietzen and Nordmann, 1987) or (San Andres, 1991), Padavala's model uses continuous functions, created by cubic splines to fit the distribution of the variables, pressure, velocity, and so forth. With this technique, it is possible to solve the bulk-flow equations for every finite part to get the pressure and velocity distribution within the seal. Although this model gives good to excellent agreement with measurements, its computational costs are high (Tiwari et al., 2005).

Further methods, based on finite volume CFD calculations like those in (Yan et al., 2015), or finite difference methods, or using the REYNOLDS equation known for journal bearings with turbulence correction factors and solved it with finite element methods, see (San Andrés and Delgado, 2012), gives high quality results.

The consequence of seal forces acting on the rotordynamics of the whole system are well described in (Gasch et al., 2006) and (Childs, 1993). The effect of self-excited vibrations and rotor instability like the "oil-whip" phenomenon are illustrated in (Muszynska, 1986) for a system with two degrees of freedom. Parametrization and variable description of the JEFFCOTT rotor model used are attributable to (Thümmel et al., 2015) and (Rossner, 2015).

Others focus on coefficient measurements using an AMB rotor system to measure transfer functions. (Zutavern, 2006) for example gets good measurement results for frequency domain identification methods. The use of a rotor seal system in journal bearings with AMB excitation, in (Gaszner, 2014), with the variation of stiffness and damping of the AMB controller leads to the rotordynamic seal coefficients for steam turbine seals.

MODELING: JEFFCOTT ROTOR MODEL

The simplified JEFFCOTT rotor model (see fig. 1) with liquid annular seals is used for theoretical explanation, simulation and as far as possible, experiments on the test rig.

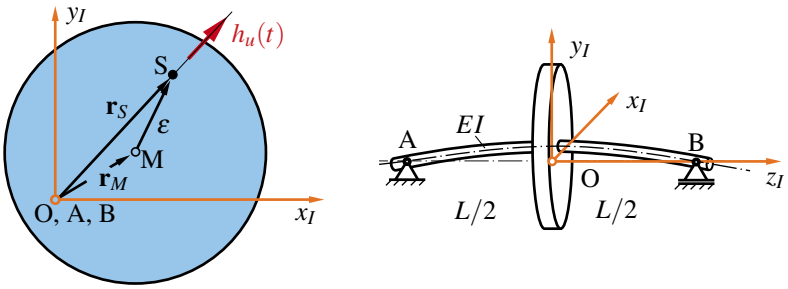

Figure 1: JEFFCOTT rotor model, parametrization according to (Thümmel et al., 2015) and (Rossner, 2015)

The JEFFCOTT rotor models a flexible, massless shaft with a mass disk symmetrically arranged between rigid bearings; see (Gasch et al., 2006). Here, the center of mass, S, has the distance ε from the disk's geometric center, M. Hence, $\mathbf{r}_M$ gives the position for M with respect to the inertial bearing connection line, A-B. $\mathbf{r}_S = \mathbf{r_M} + \varepsilon$ is the position of S in the inertial frame. Lumping the shaft stiffness, k_r, onto the rotor's center, M, and taking as degrees of freedom the two translations $\mathbf{q} = \mathbf{r}_M$ leads to dynamic equilibrium for the rotor with mass m_r:

$$\mathbf{M}\ddot{\mathbf{q}} = \sum_i \mathbf{F}_i = -\mathbf{K}\mathbf{q} + \mathbf{h} \tag{2}$$

$$\begin{bmatrix} m_r & 0 \\ 0 & m_r \end{bmatrix} \ddot{\mathbf{q}} + \begin{bmatrix} k_r & 0 \\ 0 & k_r \end{bmatrix} \mathbf{q} = \mathbf{h} \tag{3}$$

$$\mathbf{h_u} = m_r \varepsilon \Omega^2 [cos(\Omega t)\ sin(\Omega t)]^T \tag{4}$$

with the equivalent forces $\mathbf{h} = \mathbf{h_u} + \mathbf{h_e} + \mathbf{h_s}$... (unbalance, external forces, seal forces, and so forth). The rotor's natural frequency is $\omega_{crit} = \sqrt{\frac{k_r}{m_r}}$, its critical speed.

Contactless seal: Minimal model and effects on rotor system

Defining the seal as system with spring, mass, damper and coupling to the rotor using force $\mathbf{h}_s$ leads to the minimal model shown in fig. 2.

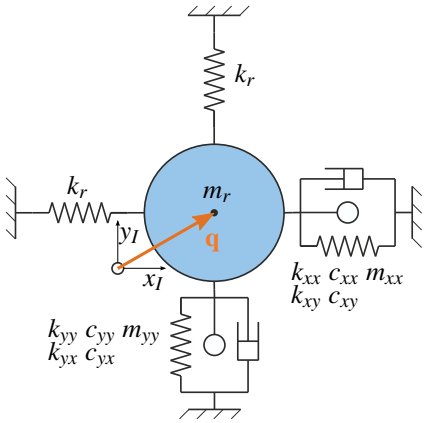

Figure 2: JEFFCOTT rotor coupled to seals

Neglecting other forces, the dynamic equilibrium for the whole rotor seal system can be written as:

$$\begin{bmatrix} m_r + m_{xx} & 0 \\ 0 & m_r + m_{yy} \end{bmatrix} \ddot{\mathbf{q}} + \begin{bmatrix} c_{xx} & c_{xy} \\ c_{yx} & c_{yy} \end{bmatrix} \dot{\mathbf{q}} + \begin{bmatrix} k_r + k_{xx} & k_{xy} \\ k_{yx} & k_r + k_{yy} \end{bmatrix} \mathbf{q} = 0 \tag{5}$$

Assuming that

$$\mathbf{q} = \hat{\mathbf{q}} e^{\lambda t} \tag{6}$$

yields the eigenvalue problem

$$\left(\lambda^2 \begin{bmatrix} m_r + m_{xx} & 0 \\ 0 & m_r + m_{yy} \end{bmatrix} + \lambda \begin{bmatrix} c_{xx} & c_{xy} \\ c_{yx} & c_{yy} \end{bmatrix} + \begin{bmatrix} k_r + k_{xx} & k_{xy} \\ k_{yx} & k_r + k_{yy} \end{bmatrix} \right) \hat{\mathbf{q}} = 0 \tag{7}$$

with eigenvalues $\lambda = \delta \pm j\omega$. For self-excited vibration, i.e. rotor instability, the positive real parts, δ, must be observed. The seal coefficients' speed dependency, mainly the increasing of cross-coupled parts of the stiffness, k_{xy} and k_{yx} , sets a speed limit for safe operation: the onset speed. A sub-synchronous, self-excited vibration at the rotor's natural frequency arises when the onset speed is reached.
Calculating the seal coefficients is essential in this case to avoid rotor instability for safe operation.

Bulk-flow modeling and seal simulation

The bulk-flow theory is derived from the NAVIER-STOKES equations by neglecting all changes to the fluid flow parameters in radial direction and setting them to constant values or zero. These assumptions lead to a pressure- and shear-driven fluid flow and a perturbation analysis about a steady state position leads to the fluid forces as a function of the rotor's movement. Simplifications made by (Black and Jenssen, 1969), (Childs, 1983) and (Padavala and Palazzolo, 1994) are used to solve the fluid momentum equations to get the rotordynamic seal coefficients. The detailed description of the used equations and the solving process is well explained in the cited literature. The three models are implemented in MATLAB and called now as Black, Childs and Padavala model. The simulation results will be discussed in later chapters.

EXPERIMENTS: TEST RIG SETUP

The test rig design is shown in fig. 3. It is based on a flexible shaft ⑨ and a mass disc ② rotating within a pressurized chamber with length l_c and clearance c_c; see ③. The shaft support is realized with stiff ball bearings ⑥ and the rig is driven by a servo motor ⑧ with the maximum speed of 6000 rpm. The fluid is injected into the chamber and flows through two symmetric annular seals ① to the environment. Two eddy current sensors ⑤ measure the rotor's motion. A dynamometer ⑦ under the stator seal is used to get the seal's reaction forces. Further, the fluid inlet pressure, temperature, rotational speed, leakage flow and torque are measured. An active magnetic bearing ④ is used as an actuator for dynamic system excitation. Tab. 1 list the test rig, the fluid and seal parameters used for simulation and measurements. Dynamic run-up behavior is shown using the waterfall plot in fig. 4. The seal influence decreases the natural frequency, which follows the unbalance response at about half rotational speed. This effect is shown by the little peak at $\Omega/2$ in fig. 4. Therefore, the rotor is always in an over-critical range above the first bending mode.

Measurement methods for seal coefficients

For a symmetrical rotor seal system, the coefficients in eq. (1) can be written, according to (Gasch et al., 2006): $M_s = m_{xx} = m_{yy}$, $C_s = c_{xx} = c_{yy}$, $c_s = c_{xy} = -c_{yx}$, $K_s = k_{xx} = k_{yy}$ and $k_s = k_{xy} = -k_{yx}$. To determine the rotordynamic seal coefficients, the seal reaction forces in eq. (1) are FOURIER transformed into the frequency domain according to

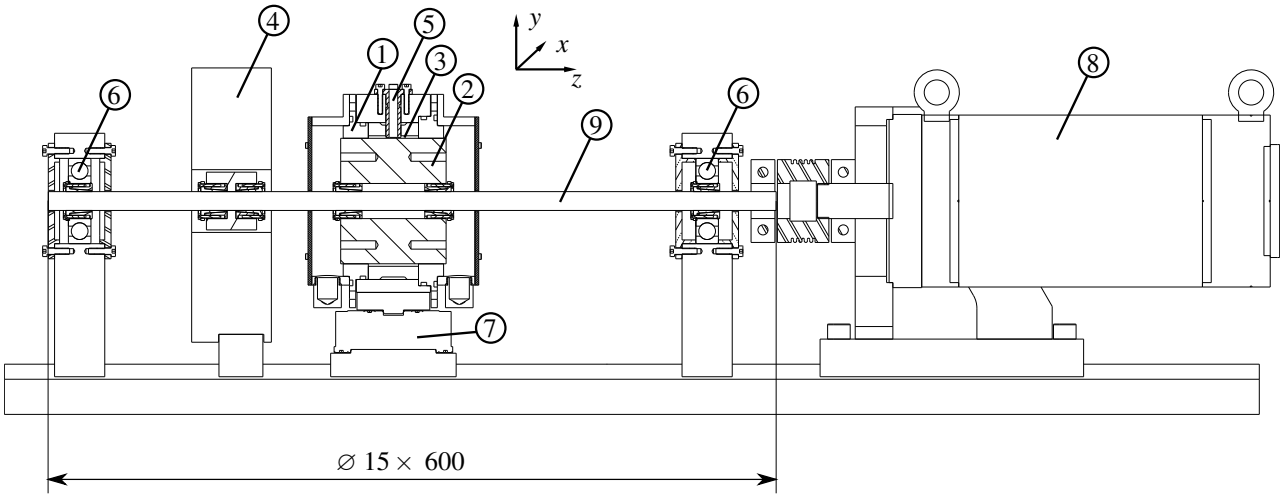

Figure 3: Seals Test Rig, see (Wagner et al., 2016)

Table 1: Test rig and seal parameters

Name	*Description*	*Value*
c	seal clearance	0.17 $[mm]$
c_c	chamber clearance	2 $[mm]$
Ω	rotational speed	0-100 $[rps]$
l	seal length	20 $[mm]$
l_c	chamber length	40 $[mm]$
Δp	pressure difference at the seals	$2{\cdot}10^5$ $[Pa]$
ν	viscosity at 40°C	0.04048 $[Pa \cdot s]$
ρ	density at 40°C	880 $[kg/m^3]$
d	seal diameter	0.1 $[m]$
m_r	rotor mass	5 $[kg]$
k_r	shaft stiffness	$2.93 \cdot 10^5$ $[N/m]$
c_r	dry damping	26.7 $[Ns/m]$
ω_0	dry natural frequency	38.6 $[Hz]$

(Massmann, 1986):

$$\underbrace{\begin{bmatrix} K_s + j\omega C_s - \omega^2 M_s & k_s + j\omega c_s \\ -k_s - j\omega c_s & K_s + j\omega C_s - \omega^2 M_s \end{bmatrix}}_{\tilde{\mathbf{A}}} \underbrace{\begin{bmatrix} \tilde{x} \\ \tilde{y} \end{bmatrix}}_{\tilde{\mathbf{q}}} = \underbrace{\begin{bmatrix} \tilde{f}_x \\ \tilde{f}_y \end{bmatrix}}_{\tilde{\mathbf{h}}_s} \tag{8}$$

$\tilde{\mathbf{A}}$ is the system's dynamic stiffness matrix for every frequency, ω, $\tilde{\mathbf{q}}$ the rotor complex displacement amplitudes, and $\tilde{\mathbf{h}}_s$ the seal complex reaction force amplitudes. Using the notation

$$\begin{aligned} a(\omega) &= K_s + j\omega C_s - \omega^2 M_s \\ b(\omega) &= k_s + j\omega c_s \end{aligned} \tag{9}$$

equation (8) becomes:

$$\begin{bmatrix} a & b \\ -b & a \end{bmatrix} \begin{bmatrix} \tilde{x} \\ \tilde{y} \end{bmatrix} = \begin{bmatrix} \tilde{f}_x \\ \tilde{f}_y \end{bmatrix} \quad \Leftrightarrow \quad \begin{bmatrix} \tilde{x} & \tilde{y} \\ \tilde{y} & -\tilde{x} \end{bmatrix} \begin{bmatrix} a \\ b \end{bmatrix} = \begin{bmatrix} \tilde{f}_x \\ \tilde{f}_y \end{bmatrix} \quad \Leftrightarrow \quad \begin{bmatrix} a \\ b \end{bmatrix} = \frac{1}{\tilde{x}^2 + \tilde{y}^2} \begin{bmatrix} \tilde{x}\tilde{f}_x + \tilde{y}\tilde{f}_y \\ \tilde{y}\tilde{f}_x - \tilde{x}\tilde{f}_y \end{bmatrix} \tag{10}$$

Eq. (10) can be solved for a and b at several excitation frequencies and for multiple measurements using a least squares method. Separation into the real part, Re, and imaginary part, Im, of a and b lets us use linear and quadratic fit curves to

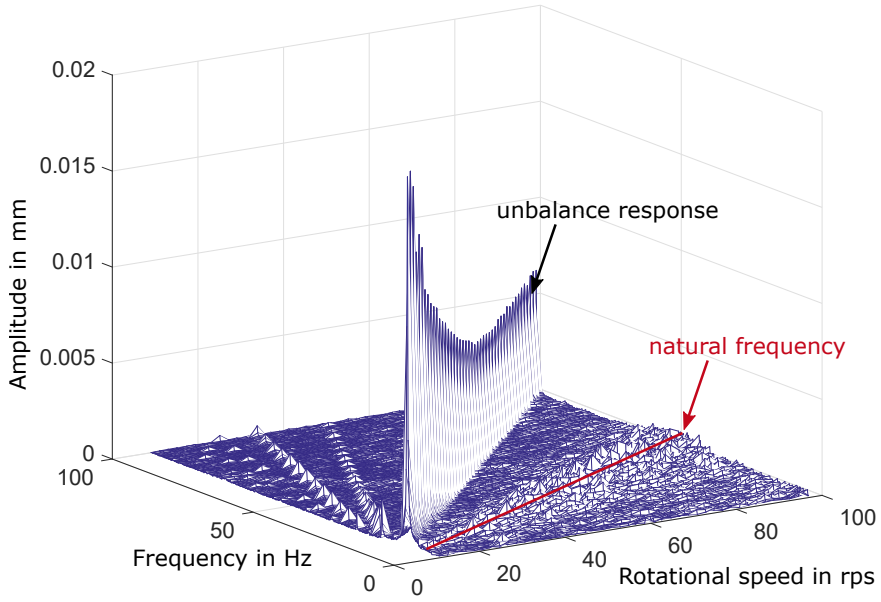

Figure 4: Waterfall plot of test-rig run up

calculate the rotordynamic coefficients:

$$\begin{aligned} Re\{a(\omega)\} &= K_s - \omega^2 M_s \\ Im\{a(\omega)\} &= \omega C_s \\ Re\{b(\omega)\} &= k_s \\ Im\{b(\omega)\} &= \omega c_s \end{aligned} \tag{11}$$

Measuring seal forces, $\tilde{\mathbf{h}}_s$, and displacements, $\tilde{\mathbf{q}}$, with one directional excitation in the y direction at several frequencies, ω, using the AMB yields the values for a and b shown in fig. 5 for the test-rig parameters in tab. 1. The blue line in fig. 5(a), which represents $Re\{a(\omega)\} = K_s - \omega^2 M_s$, should be a quadratic curve. At about 42 (rps) $\approx \Omega/2$, a discontinuous point–a "jump-effect"–disturbs the curve fitting and coefficient identification. Even when the rotational speed changes, the same noise effect occurs in every real and imaginary part of a and b at about half rotational speed; see fig 5.

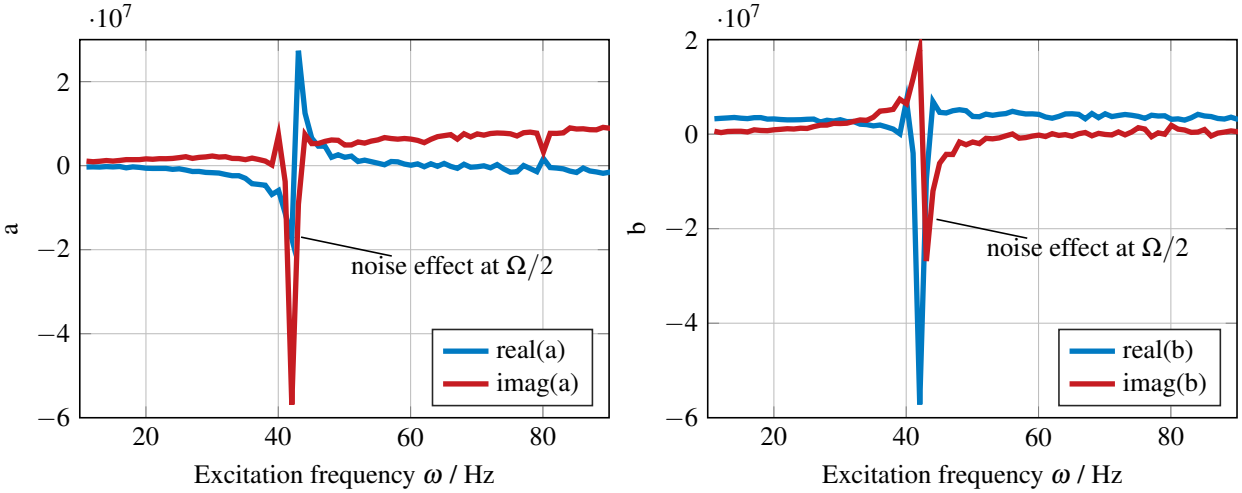

(a) $a = K_s + j\omega C_s - \omega^2 M_s$ measured at $\Omega = 80$ rps

(b) $b = k_s + j\omega c_s$ measured at $\Omega = 80$ rps

Figure 5: a and b measured in xy coordinates

Instead of using the xy coordinate system, equation (8) can be transformed to complex coordinate in the forward whirl direction $z = x + jy$ by summing up the first equation of (8) and the second equation multiplied by j, one obtains after rearranging:

$$[-\omega^2 M_s + \omega c_s + K_s + j(C_s\omega - k_s)] \cdot \tilde{z} = \tilde{f}_z \tag{12}$$

$$\frac{\tilde{f}_z}{\tilde{z}} = -\omega^2 M_s + \omega c_s + K_s + j(C_s\omega - k_s) \tag{13}$$

Separated in real and imaginary parts:

$$\begin{aligned} Re\left(\frac{\tilde{f}_z}{\tilde{z}}\right) &= -\omega^2 M_s + \omega c_s + K_s \\ Im\left(\frac{\tilde{f}_z}{\tilde{z}}\right) &= C_s\omega - k_s \end{aligned} \tag{14}$$

Figure 6 shows that fitting the rotordynamic coefficients with linear and quadratic curves is possible using the coordinate transformation. No jump effect at half rotational speed occurs in the complex coordinate description and the blue lines agree well with the dotted red quadratic and linear fitted functions. The noise at 80 Hz occurs due to the dominant unbalance force response polluting the measurement at rotational speed $\Omega = 4800\,\text{rpm}$.

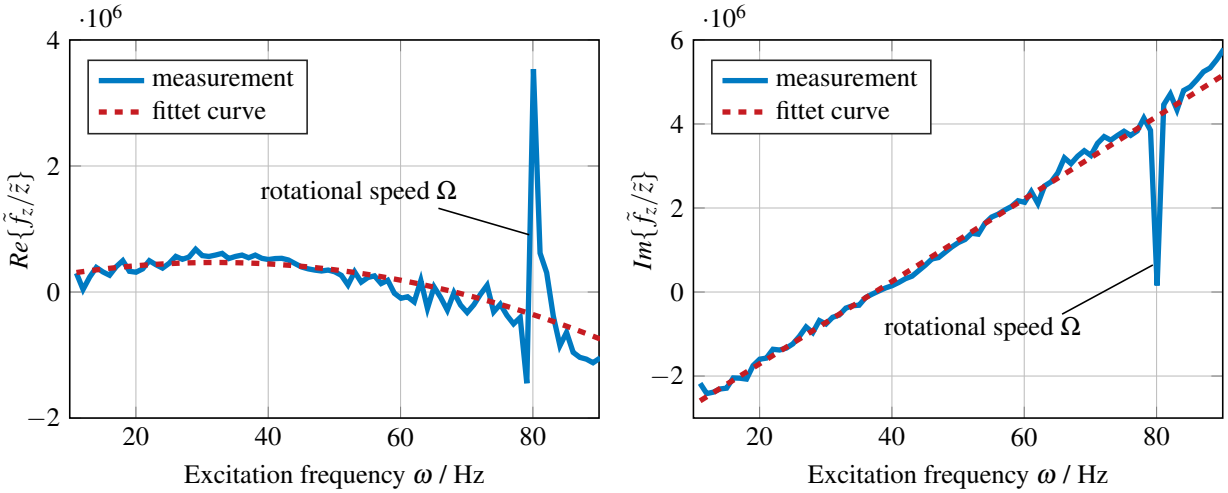

(a) Real part of $\frac{\tilde{f}_z}{\tilde{z}}$ measured at $\Omega = 80\,\text{rps}$

(b) Imaginary part of $\frac{\tilde{f}_z}{\tilde{z}}$ measured at $\Omega = 80\,\text{rps}$

Figure 6: $\frac{\tilde{f}_z}{\tilde{z}}$ measured in complex coordinate

Discussion of noise effect

The experiments show a noise effect at half rotational speed in the xy coordinate measurement. A transformation to complex coordinate solves this problem. The explanation can be found analyzing the block diagramm for equation (10), shown in fig. 7, with the unknown noise force, $\Delta\tilde{f}(t)$, acting on the rotor. The relation for the displacement errors $\tilde{\Delta}x$ and $\tilde{\Delta}y$, is given by:

$$\tilde{\Delta}x = -\frac{b}{a}\tilde{\Delta}y \qquad \text{and} \qquad \tilde{\Delta}y = \Delta\tilde{f}(t)/a \tag{15}$$

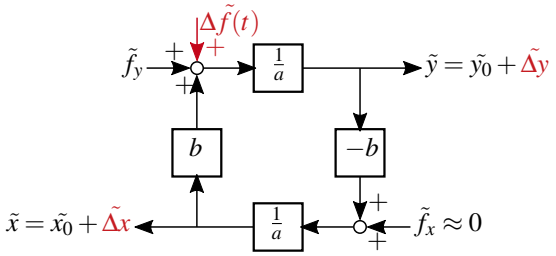

Figure 7: Block diagram of random noise influence

Using for the rotor displacement:

$$\tilde{x} = \tilde{x_0} + \tilde{\Delta}x \qquad \text{and} \qquad \tilde{y} = \tilde{y_0} + \tilde{\Delta}y \tag{16}$$

For the displacement and forces these substitutions can be done:

$$
\begin{aligned}
q &= \frac{\tilde{y}}{\tilde{f}_y} = \frac{\tilde{y_0} + \tilde{\Delta y}}{\tilde{f}_y} = q_0 + \Delta q \\
p &= \frac{\tilde{x}}{\tilde{f}_y} = \frac{\tilde{x_0} + \tilde{\Delta x}}{\tilde{f}_y} = p_0 + \frac{\tilde{\Delta x}}{\tilde{f}_y} = p_0 - \frac{b}{a}\frac{\tilde{\Delta y}}{\tilde{f}_y} = p_0 - \frac{b}{a}\Delta q \\
r &= \frac{\tilde{f}_x}{\tilde{f}_y}
\end{aligned}
\tag{17}
$$

Set into equation (10) leads to a new description for a and b:

$$
\begin{bmatrix} a \\ b \end{bmatrix} = \frac{1}{p^2 + q^2} \begin{bmatrix} p \cdot r + q \\ q \cdot r - p \end{bmatrix} \tag{18}
$$

Making the assumption $f_y \gg f_x$, $(4 \cdot 10^1 N \gg 0\ )$ and AMB excitation in y direction, so $r \approx 0$. Substitution into eq. (13):

$$
\frac{\tilde{f}_z}{\tilde{z}} = a - jb = \frac{1}{p^2 + q^2}[q + jp] = \frac{1}{p^2 + q^2}[q_0 + \Delta q + jp_0 - j\frac{b}{a}\Delta q] \tag{19}
$$

Looking back at the block diagram in fig. 7 and eq (15), it follows that

$$
\tilde{x_0} = -\frac{b}{a}\tilde{y_0} \qquad \text{and} \qquad p_0 = -\frac{b}{a}q_0 \tag{20}
$$

For the part,

$$
\frac{b}{a} = \frac{jc_s\omega + k_s}{-M_s\omega^2 + K_s + jC_s\omega} \tag{21}
$$

At around the frequency $\omega = \Omega/2$, where the former "jump effect" occurs, the assumptions $k_s \gg c_s\omega$, $(4 \cdot 10^6 N/m \gg 6 \cdot 10^5 N/m)$ and $C_s\omega \gg (-M_s\omega^2 + K_s)$, $(4 \cdot 10^6 N/m \gg 5 \cdot 10^5 N/m)$ can be made, so:

$$
\frac{b}{a} \approx \frac{k_s}{jC_s\omega} = -j\frac{k_s}{C_s\omega} \tag{22}
$$

using the rotational speed dependency of the coupled stiffness $k_s \approx C_s \cdot \Omega/2$, $(3.7 \cdot 10^6 N/m \approx 3.9 \cdot 10^6 N/m)$, $\frac{b}{a} \approx -j$ at about $\omega = \Omega/2$. So eq. (19) can be rewritten and the displacement error gets subtracted out:

$$
\frac{\tilde{f}_z}{\tilde{z}} = \frac{1}{p^2 + q^2}[q_0 + \Delta q + jp_0 - j(-j\Delta q)] = \frac{1}{p^2 + q^2}[q_0 + jp_0] \tag{23}
$$

For the fraction $\frac{1}{p^2+q^2}$ of equation (23), the displacement error is subtracted out, too:

$$
p^2 + q^2 = p_0^2 + q_0^2 + 2\Delta q(q_0 - \frac{b}{a}p_0) = p_0^2 + q_0^2 + 2\Delta q(q_0 + \left(\frac{b}{a}\right)^2 q_0) = p_0^2 + q_0^2 \tag{24}
$$

By neglecting terms of second order, $(\Delta q)^2$. The displacement error Δx and Δy due to the unknown noise force $\Delta f(t)$ can be eliminated using the complex coordinate, as shown. However, it is possible to apply this method to determine rotordynamic seal coefficients using one-directional, active magnetic bearing excitation in a flexible rotor system with additional unknown forces. The determined coefficients are needed to validate simulation models and to describe the rotor-seal system's behavior including stability prediction.

INSTABILITY PREDICTION

Simulation and eigenvalue analysis

Figure 8 shows the real and imaginary parts that result from calculating the rotor-seal system eigenvalues, $\lambda = \delta \pm i\omega$, using the simulated seal coefficients. The zero crossing of the real part gives the rotor's onset speeds of instability at about $\Omega = [160, 124 \text{ and } 136]rps$ for the three simulation models: Black, Childs and Padavala. The system's simulated natural frequency agrees with the test rig behavior at higher rotational speeds, where the natural frequency is always about half rotational speed, $\Omega/2$.

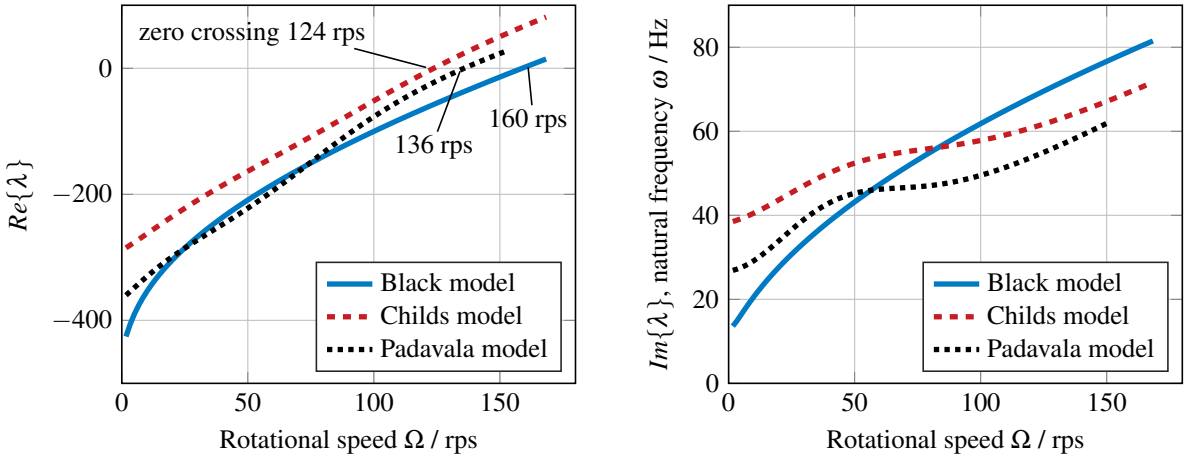

(a) Simulated real part δ of system's eigenvalue

(b) Simulated imaginary part ω of system's eigenvalue

Figure 8: Simulated eigenvalues of rotor-seal system

Coefficient measurement and experimental predictive eigenvalue analysis

The system's eigenvalues can be calculated using the measured seal coefficients and the dry test rig parameters; see fig. 9. Fig. 9(a) shows the real parts. Using "least squares" to fit a linear function to the real eigenvalues enables you to extrapolate the zero crossing and the onset speed of instability to $\Omega = 171$ rps.

Comparing the estimated onset speed shows that the experimental method predicts 38% higher rotational speed than Childs', 26% higher than Padavala's, and 7% higher than Black's simulation model. The system's natural frequency is always about $\Omega/2$ –half the rotational speed, see fig. 9(b), which agrees well with the real test rig behavior.

The measured rotordynamic seal coefficients are the blue lines shown in fig. 10. Comparing measured and simulated seal coefficients, the inertia term, mass M_s, is under predicted. The direct damping, C_s, is too low but on the same order. Direct stiffness, K_s, is over predicted but has the same shape. The trend of the cross-coupled stiffness, k_s, agrees well and is nearly linear.

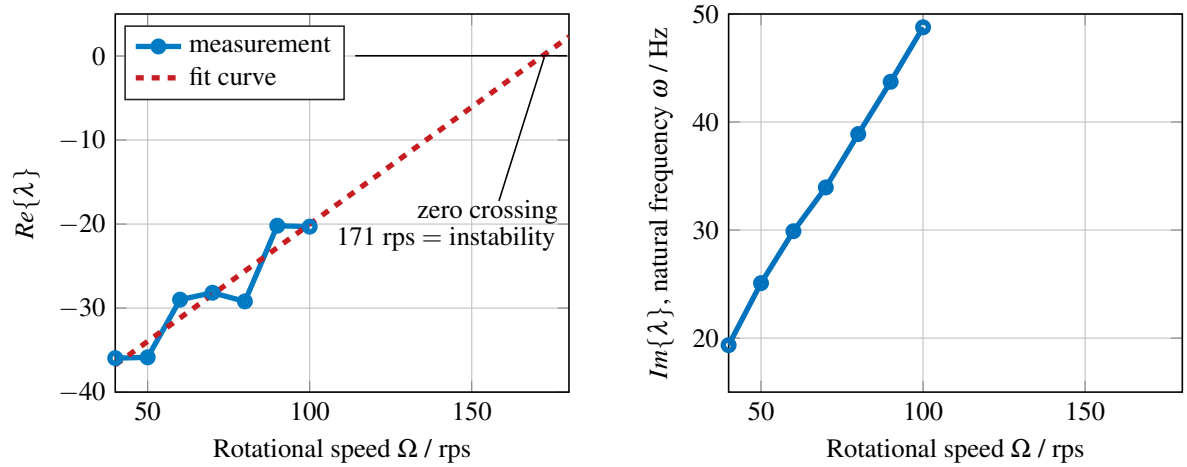

(a) Measured real part of system's eigenvalue

(b) Measured imaginary part of system's eigenvalue

Figure 9: System's eigenvalues using measured seal coefficients, experimental instability prediction

CONCLUSION

The influence of seals on rotordynamics is shown in this paper. Models from the well-known literature for calculating rotordynamic coefficients are examined and used to determine the rotor system's vibrational behavior. A test-rig design, the measurement concept, details for solving noise problems to get a robust method, and first seal coefficients are shown for model validation. The model coupling of seal and rotor leads to a prediction of the stability limit and rotordynamic behavior. Because of the early state, these are preliminary results for the test-rig and the implemented simulation models. The differences between simulated and measured seal coefficients are mostly caused by anisotropic and misalignment effects at the test rig. This is confirmed by the movement of the unloaded rotor from the complete rotor-stator contact at $\Omega = 0\,\mathrm{rps}$ nearly to the seal center at $\Omega = 100\,\mathrm{rps}$. Additional investigations to improve the test rig design and to avoid disturbances such as increasing fluid temperature, misalignment, and so forth are planned. Future works also involves increasing the rotational speed to get the real onset speed of instability. On the simulation side, improved models will be implemented for the fluid motion and the resulting forces in future.

ACKNOWLEDGMENTS

This project is supported by Ludwig Bölkow Campus and funded by the Bavarian government. Good cooperation with the consortium partners is acknowledged.

REFERENCES

Barrett, LE (1984). "Turbulent flow annular pump seals: a literature review". In: *The Shock and vibration digest* 16.2, pp. 3–13.

Black, HF and DN Jenssen (1969). "Paper 9: Dynamic Hybrid Bearing Characteristics of Annular Controlled Leakage Seals". In: *Proceedings of the Institution of Mechanical Engineers, Conference Proceedings*. Vol. 184. 14. SAGE Publications, pp. 92–100.

Childs, Dara W (1983). "Dynamic analysis of turbulent annular seals based on Hirs' lubrication equation". In: *Journal of lubrication technology* 105.3, pp. 429–436.

— (1993). *Turbomachinery rotordynamics: phenomena, modeling, and analysis*. John Wiley & Sons.

Dietzen, FJ and R Nordmann (1987). "Calculating rotordynamic coefficients of seals by finite-difference techniques". In: *Journal of Tribology* 109.3, pp. 388–394.

Gasch, Robert, Rainer Nordmann, and Herbert Pfützner (2006). *Rotordynamik*. Springer-Verlag.

Gaszner, Manuel (2014). *Rotordynamische Charakterisierung von Dichtungssystemen zur Anwendung in Kraftwerks-dampfturbinen*. Verlag Dr. Hut.

Massmann, Harald (1986). "Ermittlung der dynamischen Parameter turbulent durchströmter Ringspalte bei inkompressiblen Medien". PhD thesis.

Muszynska, Agnieszka (1986). "Whirl and whip—rotor/bearing stability problems". In: *Journal of Sound and vibration* 110.3, pp. 443–462.

Padavala, Satya and Alan Palazzolo (1994). "Enhanced simulation software for rocket turbopump, turbulent, annular liquid seals". In: *NASA Report*.

Roßner, Markus (2015). "Modellbasiertes Monitoring von Rotoren mit mehreren gleichzeitigen Fehlern". PhD thesis. München, Technische Universität München, Diss., 2015.

San Andrés, Luis Adolfo (1991). "Analysis of variable fluid properties, turbulent annular seals". In: *Journal of tribology* 113.4, pp. 694–702.

San Andrés, Luis and Adolfo Delgado (2012). "A Novel Bulk-Flow Model for Improved Predictions of Force Coefficients in Grooved Oil Seals Operating Eccentrically". In: *Journal of engineering for gas turbines and power* 134.5, p. 052509.

Thümmel, Thomas et al. (2015). "Unterscheidung verschiedener Fehlerarten beim modellbasierten Monitoring". In: *Tagungsband SIRM 2015 in Magdeburg*.

Tiwari, R, S Manikandan, and SK Dwivedy (2005). "A review of the experimental estimation of the rotor dynamic parameters of seals". In: *The Shock and vibration digest* 37.4, pp. 261–284.

Wagner, C. et al. (2016). "Rotordynamic Effects in Turbopumps". In: *Space Propulsion Conference Rome*.

Yan, Xin et al. (2015). "A Generalized Prediction Method for Rotordynamic Coefficients of Annular Gas Seals". In: *Journal of Engineering for Gas Turbines and Power* 137.9, p. 092506.

Zutavern, Z. S. (2006). "Identification of rotordynamic forces in a flexible rotor system using magnetic bearings". PhD thesis. Texas A&M University.

RESPONSIBILITY NOTICE

The authors are the only responsible for the material included in this paper.

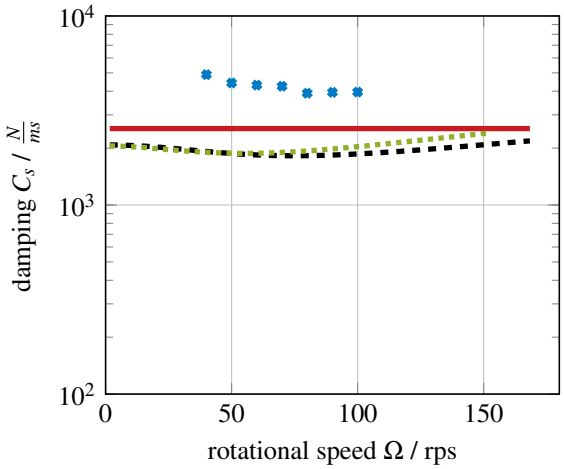

(a) Measured and simulated seal direct damping

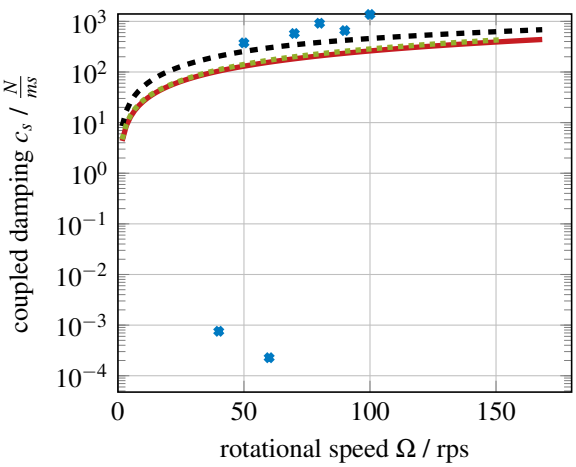

(b) Measured and simulated seal coupled damping

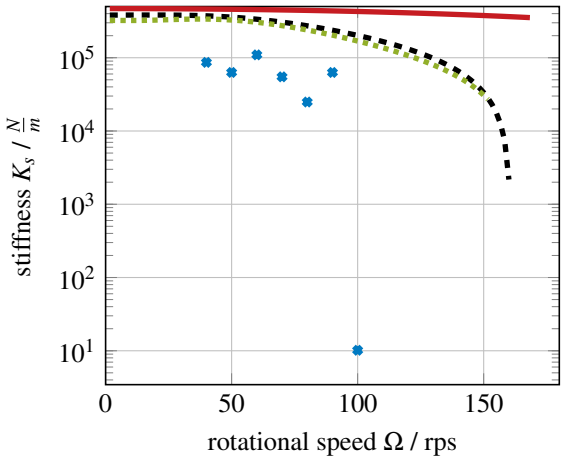

(c) Measured and simulated seal direct stiffness

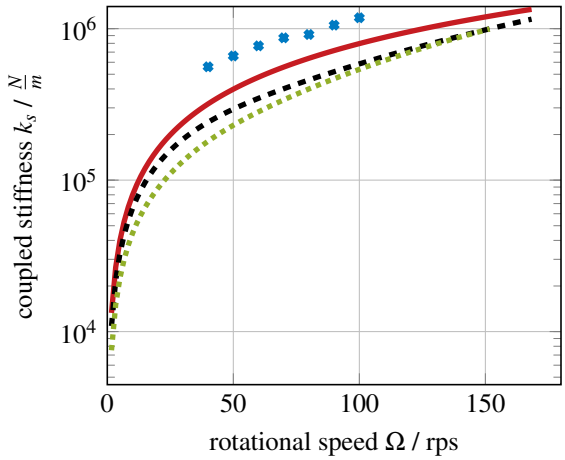

(d) Measured and simulated seal coupled stiffness

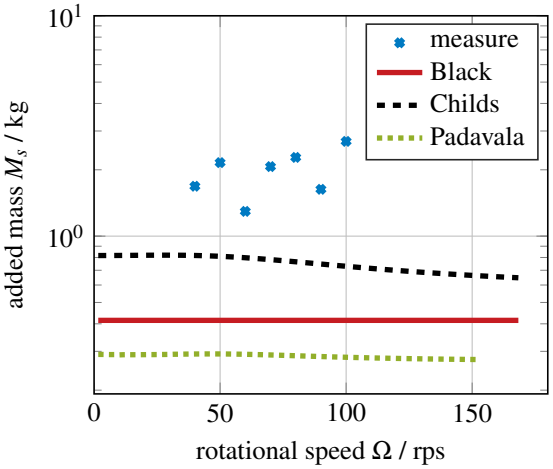

(e) Measured and simulated seal inertia

Figure 10: Simulated and measured seal coefficients